Journal of Nanoparticle Research (2007) 9:61–69
DOI 10.1007/s11051-006-9153-y

Special focus: Nanoparticles and Occupational Health

Calibration and numerical simulation of Nanoparticle Surface Area Monitor (TSI Model 3550 NSAM)

W.G. Shin[1], D.Y.H. Pui[1,*], H. Fissan[2], S. Neumann[2] and A. Trampe[2]
[1]*Mechanical Engineering Department, University of Minnesota, Minneapolis, MN, USA;* [2]*University of Duisburg-Essen, Duisburg, Germany; *Author for correspondence (E-mail: dyhpui@tc.umn.edu)*

Received 26 July 2006; accepted in revised form 1 August 2006

Key words: nanoparticle surface area, deposition in compartments of human lung, tracheobronchial, alveolar, instrumentation, occupational health

Abstract

TSI Nanoparticle Surface Area Monitor (NSAM) Model 3550 has been developed to measure the nanoparticle surface area deposited in different regions of the human lung. It makes use of an adjustable ion trap voltage to match the total surface area of particles, which are below 100 nm, deposited in tracheobronchial (TB) or alveolar (A) regions of the human lung. In this paper, calibration factors of NSAM were experimentally determined for particles of different materials. Tests were performed using monodisperse (Ag agglomerates and NaCl, 7–100 nm) and polydisperse particles (Ag agglomerates, number count mean diameter below 50 nm). Experimental data show that the currents in NSAM have a linear relation with a function of the total deposited nanoparticle surface area for the different compartments of the lung. No significant dependency of the calibration factors on particle materials and morphology was observed. Monodisperse nanoparticles in the size range where the response function is in the desirable range can be used for calibration. Calibration factors of monodisperse and polydisperse Ag particle agglomerates are in good agreement with each other, which indicates that polydisperse nanoparticles can be used to determine calibration factors. Using a CFD computer code (Fluent) numerical simulations of fluid flow and particle trajectories inside NSAM were performed to estimate response function of NSAM for different ion trap voltages. The numerical simulation results agreed well with experimental results.

Introduction

Occupational health risks associated with manufacturing and application of nanoparticles is one of the critical issues for nanotechnology development. Demands for nanomaterials are rapidly increasing, and workers may be exposed to particularly harmful nanoparticles. Several recent studies have shown that the toxicity of inhaled nanoparticles may be more appropriately associated with particulate surface area (Oberdorster et al., 1995; Oberdorster, 1996, 2005; Donaldson et al., 1998; Maynard & Kuempel, 2005). Nanoparticles defined to be below 100 nm have an increasing surface area with a decreasing particle size for the same amount of mass. From the viewpoint of nanoparticle toxicity, an instrument which measures nanoparticle surface area deposited in the human lung is very desirable.

Relatively few techniques are available to monitor exposures with respect to aerosol surface area

(Shi et al., 2001; Maynard, 2003; Jung & Kittelson, 2005). The BET method based on a gas adsorption method is not suited for a rapid evaluation of aerosol surface area at lower concentration (Brunauer et al., 1938). It can be used only for powders, not for particles in the gasborne state. It does not have on-line capabilities. The first instrument designed to measure aerosol surface-area was the epiphaniometer (Baltensperger et al., 1988). The epiphaniometer is not well suited for widespread use at the workplace because of the inclusion of radioactive source and the lack of effective temporal resolution. One of other possible methods is diffusion charging (DC). Instruments using DC include the LQ1-DC diffusion charger (Matter Engineering, Switzerland) and the TSI model 3070a Electrical Aerosol Detector (EAD). These diffusion chargers were recently evaluated (Jung & Kittelson, 2005; Ku & Maynard, 2005). Several studies using atmospheric field data have shown that EAD can be used as a useful indicator of the amount of particle surface area deposited in the lung (Woo et al., 2001; Wilson et al., 2003, 2004). Recently, it was found that response functions of EAD can be changed to match the particle surface area deposited in the lung through the adjustment of ion trap voltage in EAD (Fissan & Kuhlbusch, 2005). Based on the observation, TSI Nanoparticle Surface Area Monitor (NSAM) model 3550 has been developed to measure the nanoparticle surface area deposited in two regions, trancheobronchial (TB) and alveolar (A), of the human lung of a reference worker (Fissan et al., 2006) by adjusting ion trap voltage. Errors will occur in other cases such as kids and asthmatics; further studies are still needed for other cases. NSAM provides a simple and fast solution for measuring the surface area dose in different parts of the inhalation system.

The schematic of NSAM is shown in Figure 1. The major components of NSAM consist of a diffusion charger chamber, an ion trap, an electrometer filter, and other sharp bending parts to transport the nanoparticle stream. The total inlet flow rate of 2.5 lpm is divided into 1.5 lpm for aerosol and 1.0 lpm for sheath air surrounding a corona needle. In the charger chamber, the aerosol stream and the ion stream opposing each other are mixed. After the aerosols are charged by unipolar ions in the charger chamber, the flow with a flow rate of 2.5 lpm enters the ion trap. Excess particles with high electrical mobility and ions are removed in the ion trap. Particles which penetrate the ion trap are collected by the electrometer filter. The delivered charges give rise to a current, which is measured by an electronic circuit.

Modifications of the EAD with different ion trap voltages have been tested with the goal of determining the deposited nanoparticle surface area for different regions of the human inhalation

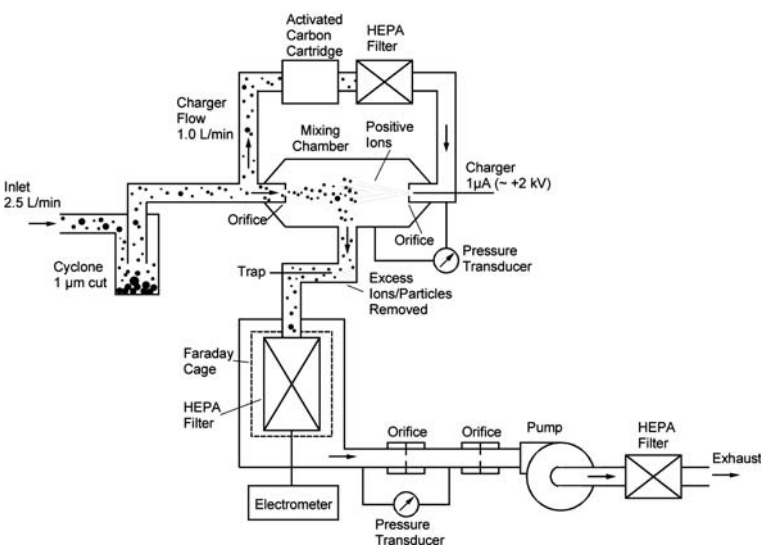

Figure 1. The schematic of NSAM.

system (Fissan & Kuhlbusch, 2005, Fissan et al., 2006). The response function curve of EAD for an ion trap voltage of 100 V matched with TB deposition and an ion trap voltage of 200 V with A deposition. The EAD with variable ion trap voltages to match the lung deposition curves is now referred as NSAM.

This paper consists of two parts. In the first part, response functions and calibration factors of NSAM for TB and A regions are experimentally obtained. The effects of particle materials and shape on the response function and calibration factor of NSAM are investigated. Tests using polydisperse and monodisperse Ag particle agglomerates are compared to each other. In the second part, numerical simulation results for the response function of NSAM are compared with experimental data.

Experimental methods

In order to obtain both the response function and the calibration curve of NSAM in which the input is the particle number concentration (N) and the output is the electrometer current (I), a test facility was constructed to generate Ag particle agglomerates with an electrical mobility size range from 7 to 100 nm (Figure 2). Ag wire (purity level 99.9 %) was placed in a ceramic boat in the furnace. Nitrogen with a flow rate of 3.0 lpm was used as a carrier gas passing through the electric furnace. The flow rate of the carrier gas was regulated by combinations of needle valve, pressure gauge, and rotameter. Silver was vaporized in the electric furnace followed by particle formation by condensation and coagulation (Han et al., 2000). Different experimental setups were added following the electric furnace depending on monodisperse or polydisperse test. In the monodisperse test, Ag particles are introduced to both an Ultrafine Condensation Particle Counter (UCPC) and NASM after primary particles are classified by a Differential Mobility Analyzer (DMA) set at a fixed voltage corresponding to particle size. In the polydisperse test, a scanning mobility particle sizer (SMPS) and UCPC are used to measure particle size distribution and polydisperse Ag particles are directly introduced to NSAM after passing through a neutralizer. For all experiments, the carrier gas flow rate was fixed at 3.0 lpm. In order to change particle size distributions, the electric furnace temperature was varied from 950 to 1200 °C. The dilution flow using compressed nitrogen gas (1.0 lpm) was also introduced in front of UCPC and NSAM. Aerosol flow after the dilution was split into two streams going into UCPC (1.5 lpm) and NSAM (2.5 lpm), respectively. For the generation of monodisperse particles, primary particles larger than the peak size of a given particle size distribution were subsequently selected with a DMA (Model 3080, TSI, Inc.). A Kr-85 neutralizer was used to get a defined charge distribution.

Experimental setup shown in Figure 2 was modified to evaluate NSAM response using NaCl

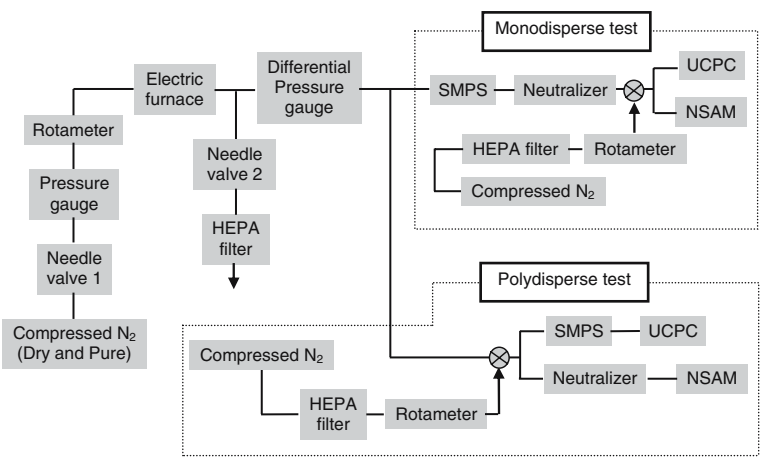

Figure 2. Experimental setup to evaluate NSAM response using monodisperse or polydisperse Ag particle agglomerates.

particles in a size range from 17 to 100 nm. A constant output atomizer (Model 3075, TSI, Inc.) was used to generate NaCl particles, and pure and dry air compressed at 37 psi was passed through the atomizer. In order to change particle size distributions, the concentration of NaCl solutions was varied from 0.0001 to 0.01 g/cc. The flow rate from the atomizer was about 3.0 lpm. Aerosol flow was passed through a diffusion dryer and then through a neutralizer to prevent particle loss due to highly charged status. In order to get higher monodispersity, primary particles larger than peak size of a given particle size distribution were subsequently selected with an electrostatic classifier (Model 3080, TSI, Inc.). In order to minimize the effect of humidity during the measurement, silica gel in the diffusion dryer was regenerated frequently. The humidity was kept as low as 30–50% during all experiments. Therefore, NaCl particles could not change in size during or after DMA classification (Tang et al., 1977). Splitting of the aerosol flow after the dilution was the same as in the case of Ag particle agglomerates.

The particle number concentration and electrometer current were simultaneously measured from UCPC and NSAM for all the experiments. The data integration time for all instruments was set to 2 min.

Normalized sensitivity and calibration factor of NSAM

For the NSAM, the input is particle number concentration (N) and the output (I) is electrometer current. Therefore, the size dependent sensitivity (S) of NSAM is given by

$$S(d_p) = \frac{I(d_p)}{N(d_p)}, \quad (1)$$

where d_p is the particle diameter. All sensitivity data are normalized with respect to the sensitivity for 100 nm particles. In other words, the sensitivity for 100 nm particles is used as a reference point. Normalized sensitivity (NS) is given by

$$NS(d_p) = \frac{S(d_p)}{S(100\,\text{nm})}. \quad (2)$$

Calibration factor of NSAM is necessary to convert NSAM electrometer current signal into nanoparticle surface area deposited in human lung. Therefore, the calibration factor (CF) is given by

$$\text{CF} = \frac{\text{Surface area deposited in human lung}}{\text{Electrometer current}}, \quad (3)$$

where CF has a unit of $\mu m^2/(cm^3 * pA)$.

Experimental results and discussion

Response function curves of NSAM for each dp^2-weighted TB or A region are shown in Figures 3 and 4, respectively. Response function curves are plotted in terms of the normalized sensitivity. It is very useful to determine how well a response function curve of NSAM is matched with an ideally wanted response function curve obtained from a theoretical lung deposition efficiency curve for TB or A region. The deposition efficiencies in TB and A regions ($\eta_{TB}$and η_A) were obtained using the UK National Radiological Protection Board's (NRPB's) LUDEP Software (James et al., 2000), based on the recommendations of ICRP Publication 66 (ICRP, 1994). The lung deposition efficiency curves of spherical nanoparticles were derived for a reference worker (Fissan et al., 2006). For particles below 100 nm, particle density has no influence on the particle lung deposition efficiency curve because the dominant mechanism of particle lung deposition is only diffusion in the size range (Heyder et al., 1986).

As shown in Figures 3 and 4, our experimental data are compared with Fissan et al. (2006) results for EAD, which is essentially the same instrument as NSAM. For Ag particle agglomerates, the two experimental data sets show good agreement with each other for both the TB and A regions. Response function curves of NSAM are well matched with those of the ideally wanted lung deposition efficiency curves for both TB and A regions. There is a small difference between Ag particle agglomerates and NaCl particles in terms of normalized sensitivity.

Even though Ag particle agglomerates below 10 nm show larger deviation from the ideally wanted response function curve in Figures 3 and 4, it has no significant contribution to integrated surface area measurement deposited in human lung because of the dp^2 dependency. The surface

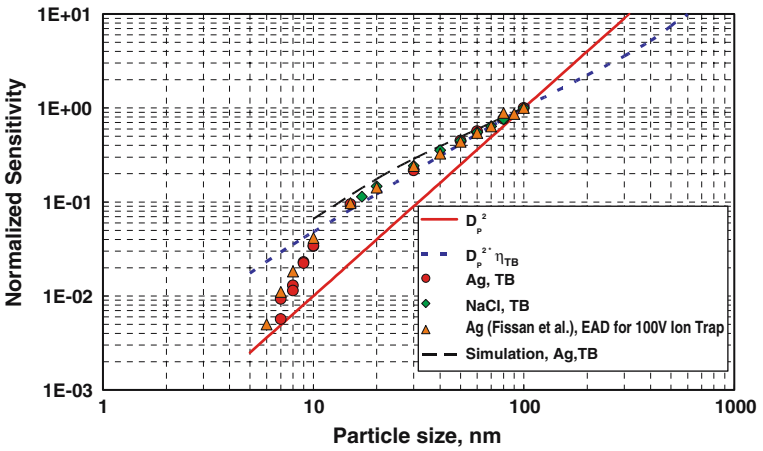

Figure 3. Comparison of response function curves of NSAM for TB region.

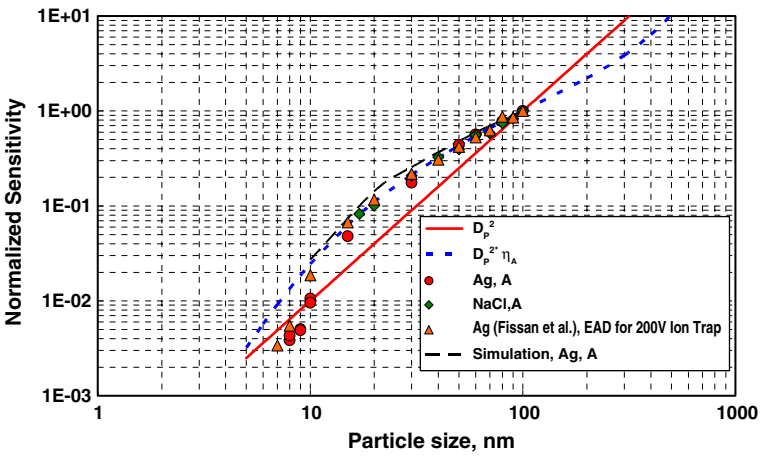

Figure 4. Comparison of response function curves of NSAM for A region.

area contribution of a 10 nm particle is only 1% of that of a 100 nm particle (Fissan et al., 2006).

Calibration curves of NSAM for TB is plotted in Figure 5. The calibration factor is obtained as the slope of the linear curve fitted to the data points on the plot for the particle surface area deposited in human lung vs. the NSAM electrometer current. Using the particle size measurement and the particle penetration efficiency, the particle surface area deposited in the human lung (DS) is calculated by

$$\begin{aligned} &\mathrm{DS}(d_\mathrm{p}) = \pi d_\mathrm{p}^2 \eta(d_\mathrm{p}) \ \text{for monodisperse particles,} \\ &\mathrm{DS} = \Sigma \pi d_\mathrm{p}^2 \eta(d_\mathrm{p}) \ \text{for polydisperse particles,} \end{aligned} \qquad (4)$$

where $\eta(d_\mathrm{p})$ is the particle lung deposition efficiency in TB or A region of human lung.

As shown in Figure 5, there exists a linear relation between the NSAM electrometer current signal and the particle surface area deposited in human lung. However, there may be a weak dependency of the calibration factor on the particle material. Calibration factors of NSAM for different parts of the inhalation system and different particle materials are summarized in Table 1. The differences of calibration factors between Ag particle agglomerates and NaCl particles are below 13% for both the TB and A regions. Several factors such as the particle morphology, the change of particle size, and particle material may have influence on this difference. However, it is believed that the first two factors have no influence on the difference of calibration factor in this experiment. Ku et al. (2005) showed that diffusion charging

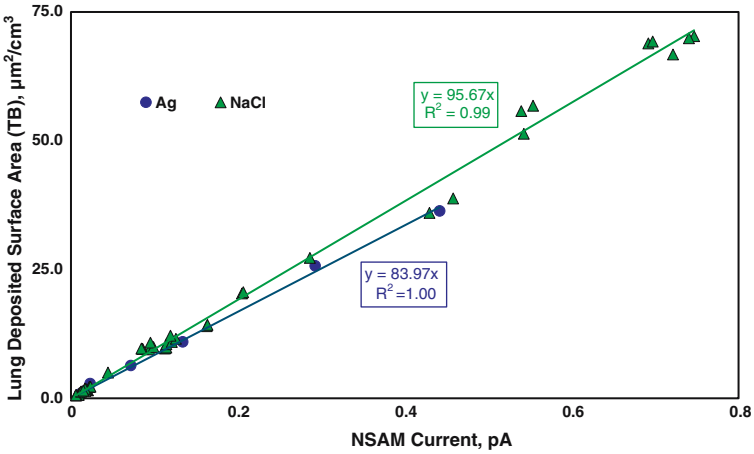

Figure 5. Calibration factor of NSAM for TB region.

Table 1. Summary of calibration factors ($\mu m^2/(cm^3$ pA)) of NSAM

Region	Ag	NaCl
TB	83.97	95.67
A	385.24	422.68

responses of the LQ1-DC (Matter Engineering, Switzerland) and DC2000CE (EcoChem, USA) were proportional to the mobility diameter squared, regardless of the morphology for monodisperse Ag particle agglomerates below 100 nm. Based on the result, the NSAM response for Ag particle agglomerates is assumed to be very close to that for spherical monodisperse Ag particle. Also, NaCl particles could not be changed in size during or after DMA classification because humidity was kept lower than the deliquescent point above which NaCl particles only can grow (Tang et al., 1977). Our data suggest that the difference of 13% between Ag particle agglomerates and NaCl particle may be attributed to the weak dependence on materials. The dielectric constant of the particle material has a second order effect on particle charging rate (Liu & Pui, 1977).

The calibration result of NSAM using polydisperse Ag particles is in agreement with that using monodisperse Ag particles for a TB region (Figure 6). It demonstrates the huge linear range of the instrument. It also demonstrates that polydisperse NaCl–aerosol can be more easily used for calibration. Therefore, any monodisperse and polydisperse aerosols can be used for the calibration purpose of NSAM for both the TB and A regions, as long as the aerosols are limited in the size range where the response function is comparable with the needed response function.

Numerical simulation results of NSAM flow path and discussion

Using a commercial CFD s/w Fluent 6.2, numerical simulations of fluid flow and particle trajectories inside NSAM were performed to estimate response functions of NSAM under different ion trap voltages. As shown in Figure 1, the geometry inside NSAM is very complex and the charging process is extremely complicated, which involves turbulent mixing of airborne particles with unipolar ions produced from a corona needle. Therefore, the model of NSAM is simplified into flow path without the diffusion charger chamber. The simplified geometry model starts from the exit of the charger chamber and ends in front of the electrometer filter. It is assumed that the exit of the charger chamber exactly matches the inlet of the ion trap. Flow variables are uniform at the inlet boundary and the inlet velocity is 2.61 m/s. Navier–Stokes equations are solved using the implicit solver in Fluent 6.2. The flow is in the laminar flow regime. The second order upwind scheme is used for the velocity equations.

Derivation of the normalized sensitivity is necessary to compare experimental data with numerical simulation results. The current signal (I)

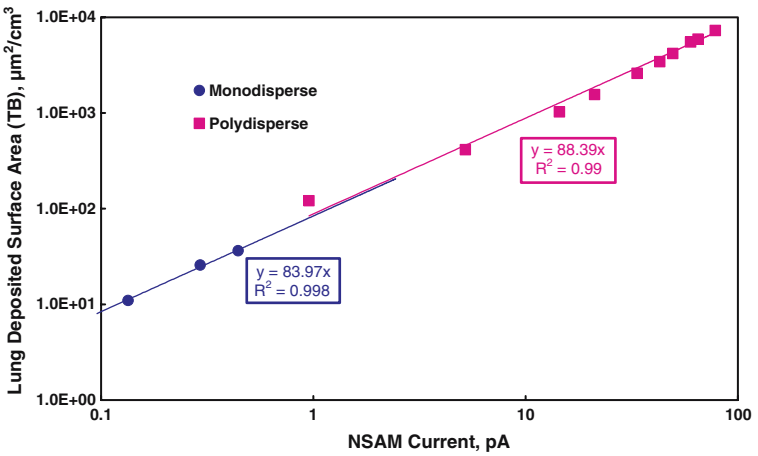

Figure 6. Comparison of calibration factors of NSAM for TB region using polydisperse and monodisperse Ag particle agglomerates.

measured by the electrometer filter inside the NSAM in the experiment is given by

$$I(d_p) = N_{in}(d_p)Q_{in}n(d_p)e\eta_{tot}(d_p), \tag{5}$$

where N_{in} is the particle number concentration at the inlet of NSAM, Q_{in} is the total flow rate (2.5 lpm) entering into the inlet of NSAM, $n(d_p)$ is the particle mean charge level, e is the charge on an electron, $\eta_{tot}(d_p)$ is the total penetration efficiency of particle in NSAM.

The mean charge level per delivered particle from diffusion charger in EAD (Medved et al., 2000; Kaufman et al., 2002), which is proportional to the particle diameter for the size range of 10–100 nm, is used in the Fluent simulations. Equation (5) is substituted into Eq. (1) and the sensitivity (S) is given by

$$\begin{aligned} S(d_p) &= \frac{N_{in}(d_p)Q_{in}n(d_p)e\eta_{tot}(d_p)}{N_{in}(d_p)} \\ &= Q_{in}n(d_p)e\eta_{tot}(d_p). \end{aligned} \tag{6}$$

Eq. (6) is substituted into Eq. (2) and the normalized sensitivity (NS) is given by

$$\begin{aligned} \mathrm{NS}(d_p) &= \frac{Q_{in}n(d_p)e\eta_{tot}(d_p)}{Q_{in}n(100\,\mathrm{nm})e\eta_{tot}(100\,\mathrm{nm})} \\ &= \frac{n(d_p)}{n(100\,\mathrm{nm})}\frac{\eta_{tot}(d_p)}{\eta_{tot}(100\,\mathrm{nm})}. \end{aligned} \tag{7}$$

The normalized sensitivity is expressed as the ratio of mean charge levels multiplied by that of total penetration efficiencies. The total penetration efficiency is given by

$$\eta_{tot}(d_p) = \eta_{\mathrm{flowpath}}(d_p) \times \eta_{\mathrm{charger\ chamber}}(d_p), \tag{8}$$

where $\eta_{\mathrm{flowpath}}(d_p)$ and $\eta_{\mathrm{charger\ chamber}}(d_p)$ are the penetration efficiencies of particles through the flow path and the charger chamber, respectively.

Equation 8 is substituted into Eq. (7) and the normalized sensitivity is given by

$$\begin{aligned} \mathrm{NS}(d_p) = \frac{n(d_p)}{n(100\,\mathrm{nm})}\frac{\eta_{\mathrm{flowpath}}(d_p)}{\eta_{\mathrm{flowpath}}(100\,\mathrm{nm})} \\ \times \frac{\eta_{\mathrm{charger\ chamber}}(d_p)}{\eta_{\mathrm{charger\ chamber}}(100\,\mathrm{nm})}. \end{aligned} \tag{9}$$

If the ratio of the penetration efficiencies for the charger chamber in the Eq. (9) is assumed to be equal to 1, the normalized sensitivity (NS) is simplified as

$$\mathrm{NS}(d_p) = \frac{n(d_p)}{n(100\,\mathrm{nm})}\frac{\eta_{\mathrm{flowpath}}(d_p)}{\eta_{\mathrm{flowpath}}(100\,\mathrm{nm})}. \tag{10}$$

The flow path penetration efficiency in Eq. (10) was obtained through particle trajectory calculations using the discrete phase model in Fluent. The effect of Brownian motion was included in the simulations. Ag particles used in Fluent simulations are in the range of 10–100 nm. In order to investigate the electrophoresis effect, a user-defined subroutine was run during the Fluent

calculation. It adds the electric force to the existing body force term of the discrete phase model in Fluent and thus enables the application of the electric field in the ion trap part. The mean charge level of particles injected from the inlet boundary is set to be proportional to the particle size in the user-defined subroutine. In each particle trajectory calculation, 1000 spherical Ag particles with the same size were released from the inlet boundary and each particle has the mean charge level proportional to its size. Material properties of Ag include a density of 10.5 kg/m^3, a thermal conductivity of 429 W/m K, and a specific heat of 235 J/kg K. The penetration efficiency for the flow path was calculated by dividing the number of particles arriving at the end point by the number of injected particles. For each particle size, the procedure of particle trajectory calculation was repeated over 20 times to improve the statistical accuracy. The normalized sensitivity was obtained by multiplying the ratio of the penetration efficiency for the flow path determined from numerical simulations by that of mean charge level as shown in Eq. (10).

A comparison of the response function curves obtained by Fluent simulation and experimental measurement can be found in Figures 3 and 4. Fluent simulation results are relatively well matched with experimental results in the size range between 10 and 100 nm. Because particles below 10 nm do not contribute significantly to the particle surface area deposited in human lung, the particles were not modeled. Normalized sensitivity estimated by Fluent simulation is larger than that obtained by experimental measurement in both cases of TB and A regions. The deviation between the model and the experimental results points to the importance of the charger chamber for the whole system. With the next version of the model, the effects within the charger chamber will be modeled.

Conclusions and discussion

We have experimentally investigated the response functions and calibration factors of a modified EAD, the TSI Model 3550 Nanoparticle Surface Area Monitor (NSAM), for the measurement of nanoparticle surface area deposited in the human lung. Also, we have analytically derived normalized sensitivity of the NSAM to compare experimental data with numerical simulation results. The comparison indicates that numerical simulation is a valuable method to predict the NSAM results.

NSAM shows a linear relation between the particle surface area deposited in human lung and the electrometer current for both TB and A regions of a reference worker. The results look promising in that NSAM gives a real-time quantitative measurement of the particle surface area deposited the human lung and thus can be used to correlate with epidemiological studies for nanoparticles below 100 nm. From the experimental data, there is a weak dependency of response function curves of NSAM on particle materials. Also, the NSAM calibration factors for both the TB and A regions show a weak dependency on particle materials. The differences between Ag particle agglomerates and NaCl particles are below 13%. For calibration, monodisperse nanoparticles in the size range where the response function is in the desirable range can be used. Polydisperse nanoparticles can be used more easily for the calibration purpose.

Fluent simulations results matched reasonably well with experimental results in terms of the response function. It demonstrates that Fluent simulation can be used to optimize the NSAM response qualitatively. However, in order to get more accurate results quantitatively from numerical simulation, the charger chamber penetration efficiency also needs to be considered in the numerical simulations. Furthermore, it is suggested that modification of ion trap configurations can be considered to improve the match between the response function of NSAM and the ideally wanted response function curve.

Acknowledgements

The authors wish to acknowledge the University of Minnesota Supercomputer Institute for providing the computation time for this project.

References

Baltensperger U., H.W. Gäggeler & D.T. Jost, 1988. The epiphaniometer, a new device for continuous aerosol monitoring. J. Aerosol Sci. 19(7), 931–934.

Brunauer S., P.H. Emmett & E. Teller, 1938. Adsorption of gases in multimolecular layers. J. Am Chem. Soc. 60, 309–319.

Donaldson K., X.Y. Li & W. MacNee, 1998. Ultrafine (nanometer) particle mediated lung injury. J. Aerosol Sci. 29(5–6), 553–560.

Fissan H. & T. Kuhlbusch, 2005. Strategies and instrumentation for nanoparticle exposure control in air at workplaces. 2nd International symposium on nanotechnology and occupational health, Minneapolis, USA, October 3–6, 2005.

Fissan H., A. Trampe, S. Neunman, D.Y.H Pui & W.G. Shin, 2006. Rationale and principle of an instrument measuring lung deposition area. J. Nanoparticle Research (this issue).

Han H.S., D.R. Chen, B.E. Anderson & D.Y.H. Pui, 2000. A nanometer aerosol size analyzer (nASA) for rapid measurement of high concentration size distributions. J. Nanoparticle Res. 2, 43–52.

Heyder J., J. Gebhart, G. Rudolf, C.F. Schillerd & W. Stahlhofen, 1986. Deposition of particles in the human respiratory tract in the size range 0.005–15μm. J. Aerosol Sci. 17, 811–825.

ICRP., 1994. International Commission on Radiological Protection Publication 66 Human Respiratory Tract Model for Radiological Protection. Oxford, Pergamon: Elsevier Science Ltd.

James A.C., M.R. Bailey & M-D. Dorrian, 2000. LUDEP Software, Version 2.07: Program for implementing ICRP-66 Respiratory tract model. RPB, Chilton, Didcot, OXON. OX11 ORQ UK.

Jung H.J. & D.B. Kittelson, 2005. Characterization of aerosol surface instruments in transition regime. Aerosol Sci. Tech. 39(9), 902–911.

Kaufman S.L., A. Medved, A. Pöcher, N. Hill, R. Caldow & F.R. Quant, 2002. An electrical aerosol detector based on the corona-jet charger. AAAR conference (poster).

Ku B.K. & A.D. Maynard, 2005. Generation and investigation of airborne Ag nanoparticles with specific size and morphology by homogeneous nucleation, coagulation and sintering. J Aerosol Sci. 36(9), 1108–1124.

Liu B.Y.H. & D.Y.H. Pui, 1977. On unipolar diffusion charging of aerosols in the continuum regime. J. Colloid Interface Sci. 58, 142–149.

Maynard A.D. & E.D. Kuempel, 2005. Airborne nanostructured particles and occupational health. J. Nanoparticle Res. 7(6), 587–614.

Maynard A.D., 2003. Estimating aerosol surface area from number and mass concentration measurements. Ann. Occup. Hygiene 47, 123–144.

Medved A., F. Dorman, S.L. Kaufman & A. Pöcher, 2000. A new corona-based charger for aerosol particles. J. Aerosol Sci. 31(S.1), 616–617.

Oberdorster G., R.M. Gelein, J. Ferin & B. Weiss, 1995. Association of particulate air pollution and acute mortality: involvement of ultrafine particles. Inhal. Toxicol. 7, 111–124.

Oberdorster G., 1996. Significance of particle parameters in the evaluation of exposure-dose-response relationships of inhaled particles. Particulate Sci. Technol. 14(2), 135–151.

Oberdörster G., E. Oberdörster & J. Oberdörster, 2005. Invited review: nanotechnology: an emerging discipline evolving from studies of ultrafine particles. Environ. Health Perspect. 113(7), 823–839.

Shi J.P., R.M. Harrison & D. Evans, 2001. Comparison of ambient particle surface area measurement by epiphaniometer and SMPS/APS. Atmos. Environ. 35(35), 6193–6200.

Tang I.N., H.R. Munkelwitz & J.G. Davis, 1977. Aerosol growth studies—II. Preparation and growth measurements of monodisperse salt aerosols. J. Aerosol Sci. 8(3), 149–159.

Wilson W.E., H.-S. Han, J. Stanek, J. Turner & D.Y.H. Pui, 2003. The Fuchs surface area measured by charge acceptance of atmospheric particles may be a useful indicator of the quantity of particle surface area deposited in the lung. Abstracts of the European aerosol conference. S421-S422. Madrid, Spain.

Wilson W.E., H.-S. Han, J. Stanek, J. Turner, D.-R. Chen & D.Y.H. Pui, 2004. Use of electrical aerosol detector as an indicator for the total particle surface area deposited in the lung. Symp. On air quality measurement methods and technology sponsored by air and waste management association. Research triangle park, NC. Paper #37.

Woo K.-S., D.-R. Chen, D.Y.H. Pui & W.E. Wilson, 2001. Use of continuous measurements of integral aerosol parameters to estimate particle surface area. Aerosol Sci. Tech. 34, 57–65.